Applied Surface Science 712 (2025) 164217

Contents lists available at ScienceDirect

Applied Surface Science

journal homepage: www.elsevier.com/locate/apsusc

Full Length Article

Indentation-induced formation of vacancy defects in β-Ga_2O_3 crystals

Curtis P. Irvine [a], Billy J. Murdoch [b], Matthew R. Field [b], Fatima Matar [a], Matthew R. Phillips [a], Cuong Ton-That [a,*]

[a] School of Mathematical and Physical Science, University of Technology, Sydney, Ultimo, NSW 2007, Australia
[b] RMIT Microscopy and Microanalysis Facility, STEM College, RMIT University, Melbourne, VIC 3001, Australia

ARTICLE INFO

Keywords:
Monoclinic Ga_2O_3
Spherical indentation
Deformation
Vacancy defects
Cathodoluminescence imaging
EBSD

ABSTRACT

This study investigates the near-surface mechanical behavior and defect formation in (−201) β-Ga_2O_3 crystals subjected to spherical nanoindentation. Nanoindentation load-displacement measurements identify pop-in events at applied loads of 8 mN or higher, marking the onset of elastic-plastic deformation. Mechanical characterisation provides depth-dependent hardness and Young's modulus values, ranging from 2 to 23 GPa and from 99 to 380 GPa, respectively. Cathodoluminescence (CL) spectroscopy shows a 270 meV redshift and intensity enhancement of blue luminescence (BL) due to donor–acceptor pair (DAP) transitions involving oxygen vacancies (V_O) and gallium vacancy (V_{Ga} or V_O-V_{Ga} complexes), accompanied by strong quenching of the intrinsic UV emission associated with self-trapped holes. These spectral changes are attributed to the formation of vacancy defects and extended non-radiative recombination centers during the pop-in event. Depth-resolved CL spectroscopy and spectral mapping reveal that these defects extend well beyond the indenter contact zone, while complementary electron backscatter diffraction (EBSD) mapping confirms localized plastic deformation and dislocation activity around the indent perimeter. The findings provide direct evidence that dislocation motion under mechanical stress generates both radiative and non-radiative defects in β-Ga_2O_3, highlighting its susceptibility to mechanical damage in optoelectronic and power electronic devices.

1. Introduction

Gallium oxide (Ga_2O_3) is an emerging semiconductor with significant potential for next-generation deep UV optoelectronic and high-efficiency power electronic devices. Its ultrawide ~4.8eV bandgap, excellent chemical and thermal stability and high breakdown field (~8MV/cm) distinguish it from conventional semiconductors like Si and GaN [1,2]. Fabrication processes such as polishing, cleaving and handling often introduce large mechanical stresses, inducing plastic deformation in semiconductors, leading to plastic deformation accompanied by the formation of dislocations, stacking faults, vacancies and interstitials [3–5]. These point and extended defects can adversely affect the optical and electrical properties as they alter carrier densities by generating carriers, passivating dopants, and affecting carrier transport through carrier trapping and scattering. Moreover, extended structural defects typically act as competitive non-radiative carrier recombination centres, efficiently quenching radiative luminescence mechanisms [2,3]. Photoluminescence (PL) and cathodoluminescence (CL) spectroscopy measurements of β-Ga_2O_3 single crystals reveal a broad emission spectrum consisting of a UV band at 3.3eV and broad blue luminescence (BL) emission band at 2.8 eV; these two CL bands are attributed to the radiative relaxation of self-trapped holes and donor–acceptor pair (DAP) transitions, respectively [6–8]. There is broad agreement that the BL in high-purity Ga_2O_3 crystals originates from deep oxygen vacancy (V_O) donors and deep gallium vacancy (V_{Ga}) acceptors or (V_O-V_{Ga}) di-vacancy acceptor complexes because of the large ~ 2 eV red-shift of the BL relative to the bandgap energy [9,10]. Moreover, the intensity of the BL has been directly correlated with higher concentrations of V_{Ga} [9].

The stable β-phase of Ga_2O_3 possesses monoclinic structure and belongs to the C2/m space group. Among its crystallographic planes, the (−201) plane exhibits the highest critical load for the elastic–plastic transition, whilst the (010) plane has the lowest, rendering it the most brittle [11,12]. The elastic modulus and hardness are comparable for the (−201) and (001) planes, with typical values of approximately 180GPa and 10GPa, respectively, but are notably lower for the (010) plane [12,13]. Nanoindentation serves as a powerful tool for investigating the mechanical properties and deformation mechanisms of materials, allowing precise measurement of hardness, elastic modulus and plastic

* Corresponding author.
E-mail address: Cuong.Ton-That@uts.edu.au (C. Ton-That).

https://doi.org/10.1016/j.apsusc.2025.164217
Received 1 February 2025; Received in revised form 22 July 2025; Accepted 30 July 2025
Available online 4 August 2025

deformation under controlled loads [14]. Recent studies employing nanoindentation on β-Ga_2O_3 have reported the formation of various defect types under mechanical stress, including native point defects, stacking faults, twinning structures and dislocations [3,12]. While the mechanical deformation and defect formation in ultra-wide bandgap semiconductors such as ZnO and GaN have been extensively studied [15–17], similar investigations into β-Ga_2O_3 are currently limited. Mechanical deformation in semiconductors is known to introduce native point and extended defects, which can act as non-radiative recombination centers, significantly quenching luminescence [18]. However, in some cases, deformation-related defects enhance specific emissions, such as the yellow luminescence in ZnO [15]. For other materials, nanoindentation studies have demonstrated the anisotropic generation of defects. For example, Wigner-Seitz cell analysis of nano-indented Mg revealed the anisotropic formation of vacancy defects influenced by interplanar spacings [19]. Similarly, optoelectronic studies of mechanically induced defects in SiC revealed emission bands attributed to silicon vacancies [20]. Luminescence investigations of GaN have shown that mechanical deformation quenches band-to-band recombination while enhancing defect-related emissions associated with V_{Ga} defects [4,21,22]. To date, to the best of our knowledge, the formation of point defects in Ga_2O_3 induced by nanoindentation remains largely unexplored, leaving a significant gap in understanding its optical behaviour under mechanical stress. During the nanoindentation loading, displacement bursts, known as pop-ins, are commonly attributed to phase transformations or the nucleation of dislocations during the transition from elastic to elastic–plastic deformation [23,24]. Comparison of the defect-related CL spectra in materials such as ZnSe and GaN before and after pop-in events have shown that that changes in CL defect emissions occur only after these events, indicating dislocation nucleation is accompanied by the generation of point defects [4,18,25].

In this study, spherical nanoindentation experiments with loads up to 10mN were conducted to investigate the mechanical properties and stability of bulk (−201) β-Ga_2O_3 crystals. No evidence of pressure-induced phase transformations was observed in the mechanically damaged regions. Pop-in events occurred at indenter loads exceeding 8 mN, marking the onset of dislocations and stacking fault formation accompanied by the formation of V_O and V_{Ga} defects. The extended defects were found to strongly quench the overall CL, particularly the UV emission. In contrast, the formation of vacancy defects enhanced the BL relative to the UV, supporting its attribution to deep donor–deep acceptor pairs, involving V_O donors and V_{Ga} or (V_{Ga}-V_O) acceptors.

2. Experimental details

Nanoindentations were performed on a (−201) β-Ga_2O_3 single crystal (Tamura Corporation, Japan) using a Hysitron TI950 TriboIndenter equipped with a spherical diamond indenter of 1 μm in diameter. Maximum loads of 0.2, 2, 4, 6, 8, 9, and 10 mN were applied. During each indentation cycle, the applied load, P, was linearly increased from zero to the maximum load value over a 5 s interval, followed by a 2 s hold at the maximum load before unloading. Indentation sites were examined using Atomic Force Microscopy (AFM, Park XE7) in non-contact mode. Confocal Raman spectra were acquired in the backscattering geometry using a Horiba LabRAM HR Evolution Raman spectrometer with a 532nm laser line. Spectral CL mapping was conducted using an FEI Quanta 200 Scanning Electron Microscope (SEM) equipped with a custom-built hyperspectral CL imaging and spectroscopy system. The CL setup incorporated a parabolic mirror for CL light collection and Ocean Optics QE65000 spectrometer [26]. As the electron beam scanned across the sample, a full CL spectrum was recorded per pixel, generating a 3D hyperspectral dataset. Monochromatic CL maps were extracted to analyze spatial emission variations, particularly at photon energies of 3.34eV (STH emission) and 2.88eV (defect-related emission). Temperature dependent CL measurements were performed using a Gatan liquid nitrogen temperature-controlled cryostat stage, with all spectra corrected for the total system response of the CL system. Monte Carlo simulations of electron-solid interactions were performed using the CASINO v2.48 software package, with the CL probe depth defined as the depth at which 70 % of the electron energy loss occurred [27]. Electron backscatter diffraction (EBSD) was employed to examine the microstructural response of β-Ga_2O_3 around the indents using kernel average misorientation (KAM) and inverse pole figure (IPF) imaging. KAM processing was used to visualize local lattice strain and plastic deformation by mapping deviations in the crystal lattice orientation, while IPF maps provided information on crystallographic orientation relative to the surface normal. The EBSD measurements were performed using a JEOL JSM-7200F SEM equipped with an Oxford Symmetry EBSD detector, operated at 20kV and 1nA. During EBSD mapping, the crystal was positioned with a working distance of approximately 10 mm and tilted at 70°.

3. Results and discussion

Fig. 1 illustrates the load–displacement (P-h) curves for the β-Ga_2O_3 crystal under applied loads of 0.2, 2, 4, 8, 9 mN and 10mN. Key indentation parameters, including the maximum indenter depth (h_{max}), contact depth (h_c), and final residual depth (h_f) are indicated in Fig. 1(f) and schematically depicted in Fig. 2(a). All six P-h curves exhibit a distinct separation between their loading and unloading profiles. This separation arises because the loading phase involves both elastic and plastic deformation, whereas the unloading phase is governed solely by elastic recovery. For applied loads from 0.2 to 4mN [Fig. 1(a, b, c)], the P-h curves exhibit smooth loading and unloading profiles without any discernible discontinuities. In this range, h_{max} increases from 36 to 103nm, while h_f rises from 28 to 57nm. At higher applied loads of 8, 9 and 10mN, pop-in events occur during the loading phase at displacements of 103, 123 and 124nm, respectively. The variation in pop-in onset is attributed to local differences in surface quality and the inherently stochastic nature of dislocation nucleation, consistent with previous nanoindentation studies [3,28,29]. The magnitude of these pop-in excursions increases with higher loads, resulting in greater penetration depths. Further insights into the deformation behavior are provided in Fig. S1, which shows AFM images of the surface indents created under a 4mN (no pop-in) and a 9 mN (with pop-in) loads. Both indents, with depths ranging from 20 to 30nm, are clearly resolved. Notably, no evidence of slip bands is observed in the β-Ga_2O_3 crystal, contrasting with deformation behaviors in more symmetric crystals such as ZnO [5]. This highlights the unique deformation mechanism of β-Ga_2O_3, attributable to its anisotropic monoclinic structure.

The elastic modulus and hardness of the Ga_2O_3 crystal are analyzed according to the Oliver-Pharr method [30,31]. In this method, the contact stiffness, S, is derived from the gradient of the unloading curve:

$$S = \frac{dP}{dh} = \frac{2}{\sqrt{\pi}} E_R \sqrt{A} \tag{1}$$

where E_R is reduced elastic modulus and A is the contact area of the indenter tip. For a spherical indenter, $A = 2\pi R h_c$, with $R = 500$ nm and the contact depth $h_c = (h_{max} + h_f)/2$, as shown in Fig. 2(a) [31,32]. The elastic modulus, E, can then be determined from the experimentally determined reduced elastic module, E_R, by [31,32]:

$$\frac{1}{E_R} = \frac{(1-\nu_i^2)}{E_i} + \frac{(1-\nu^2)}{E} \tag{2}$$

where E_i and ν_i are the Young's modulus and Poisson's ratio of the diamond indenter ($E_i = 1140$GPa, $\nu_i = 0.07$), and E and ν are the corresponding properties of β-Ga_2O_3. The hardness, H, is calculated as $H = \frac{P_{max}}{A}$, where P_{max} is the maximum applied load. The calculated values of E and H are presented in Fig. 2(b). The hardness of the β-Ga_2O_3 crystal increases from 2 to 23 GPa as the penetration depth increases from 30 to

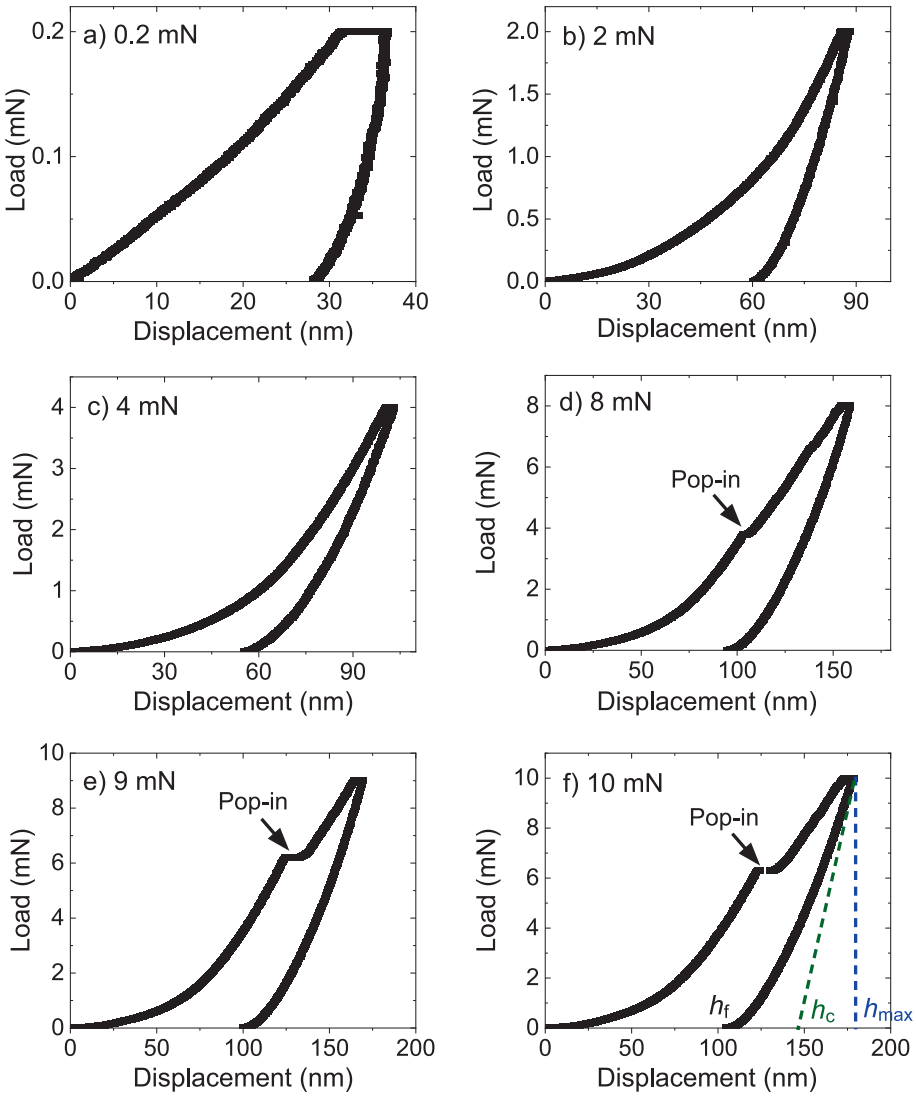

Fig. 1. Load-displacement (P-h) curves for the β-Ga_2O_3 crystal under indentation loads of 0.2, 2, 4, 8, 9 and 10 mN. Pop-in events are observed at loads at 8 mN and higher, indicating the onset of plastic deformation. Panel (f) illustrates key indentation parameters: h_f (final residual depth), h_c (contact depth) and h_{max} (maximum penetration depth).

180nm, while the elastic modulus rises from 99 to 380 GPa. These values fall within the wide ranges of reported mechanical properties of β-Ga_2O_3, where hardness varies from 2 to 35 GPa and elastic modulus spans 40 to 400 GPa [11,33,34]. The observed increase in both *E* and *H* with penetration depth is consistent with the indentation size effect reported for crystalline materials under spherical contact conditions [29,35]. At shallow depths, deformation remains partially elastic and the measured hardness primarily reflects the mean contact pressure. As penetration increases, geometrically necessary dislocations accumulate and a plastic zone develops, leading to a gradual rise and eventual saturation in *E* and *H*.

Fig. 3 presents the CL spectra of pristine β-Ga_2O_3 and sites indented with 4mN and 9mN loads. Prior CL studies have established that β-Ga_2O_3 exhibits an intrinsic ultraviolet (UV) emission near 3.3 eV due to self-trapped holes (STHs) and a broad blue luminescence (BL) band at 2.8–2.9 eV associated with DAP recombination involving oxygen vacancies (V_O) as donors and gallium vacancies (V_{Ga}) or V_{Ga}–V_O complexes as acceptors [6,9,36]. At the 4mN indentation site, where no pop-in event occurs, the normalized CL spectra show no changes in peak position or line shape before and after indentation at either 88K or 300K [Fig. 3(a, c)], indicating the absence of newly formed radiative centres. The insets within Fig. 3(a, c) display the as-measured CL spectra, revealing modest luminescence reductions by factors of 1.1 (88K) and 1.2 (300K), attributed to minor non-radiative defect formation. In contrast, the 9mN indentation site, associated with a pop-in event, exhibits a pronounced spectral transformation. At 300K, the CL spectrum redshifts by 270meV [Fig. 3(d)], with the 2.92eV BL emission dominating. This spectral shift and emission intensity enhancement are consistent with an increased density of V_O and V_{Ga}-related DAP centers formed during dislocation activity. These defects enhance the vacancy-related DAP BL emission, which dominates over the thermally quenched STH UV emission at room temperature [9], resulting in the CL spectrum predominantly characterized by the BL emission, peaking at 2.92eV. At 88K, the pristine and indented spectra are largely similar, with the STH UV emission remaining dominant; however, a small redshift and enhanced BL intensity confirm the formation of vacancy defects. The insets in Fig. 3(b, d) display the as-measured CL spectra at the 9mN site, revealing a substantial decrease of the CL intensity by factors of 2.7 (88K) and 10.9 (300K). These reductions signify to the introduction of efficient non-radiative recombination pathways, most likely associated with dislocations generated during the pop-in event [37]. Such extended defects are well-known to act as non-radiative centers by facilitating carrier capture and recombination involving phonon relaxation without photon emission, thereby suppressing the intrinsic UV emission

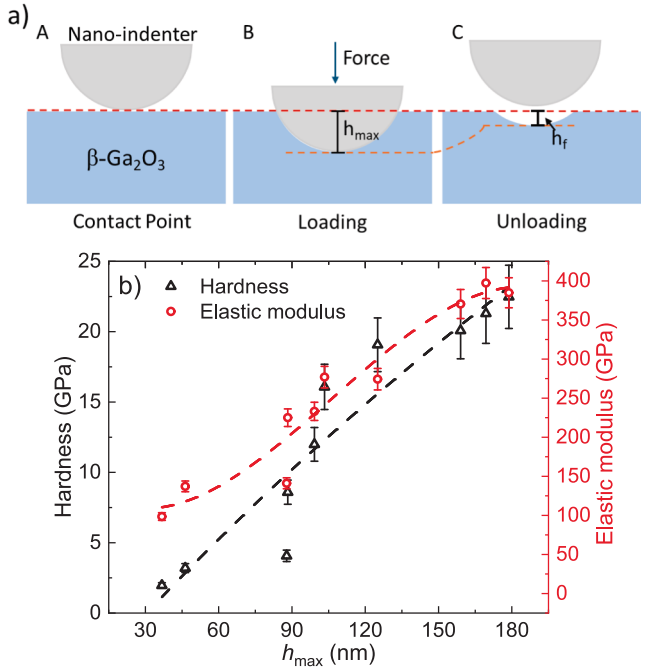

Fig. 2. (a) Schematic illustrating the three indentation cycle stages for a (−201) β-Ga_2O_3 single crystal on a hard substrate: contact (A), loading (B) and unloading (C). The schematic shows h_{max} in stage B and h_f in stage C. (b) Calculated hardness (H) and elastic modulus (E) of the Ga_2O_3 crystal as functions of h_{max}.

associated with self-trapped holes [37]. Previous nanoindentation studies on (−201) β-Ga_2O_3 crystals under similar loads have reported dislocation formation along (101) lattice planes [3], and dangling bonds along these extended structural dislocations are well known to characteristically act as non-radiative recombination centers, suppressing luminescence [38]. As seen in Fig. 3, the quenching of CL emission is particularly pronounced at 300 K, consistent with the activation of non-radiative recombination channels at elevated temperatures [39,40]. In contrast, indentation loads below 8mN, where no pop-in occurs, produce neither significant spectral shifts nor enhanced BL emission, further confirming that defect generation is driven by dislocation activity rather than thermal diffusion. Similar correlations between pop-in-induced dislocation nucleation and vacancy defect formation have been reported in mechanically stressed GaN and ZnO crystals [15,28,41].

Fig. 4(a) presents the monochromatic CL intensity maps of the 9mN indented site for the UV emission at 3.34 eV and the BL emission at 2.86 eV. Both maps are derived from the same hyperspectral scan, minimizing external perturbations and enabling direct comparison of spatial emission distributions. The concurrently acquired SEM image shows the surface morphology of the same region, including a visible indentation mark that corresponds precisely to the CL mapping area. Significant intensity variations across the indented region are observed: the areas of highest plastic deformation, indicated by the darkest areas, occur both inside and outside the contact zone, while structurally damaged regions with low CL intensity extend well beyond the indenter footprint.

The spatial correlation between the STH and BL maps indicates that indentation-induced defects suppress both STH and BL emissions. The depth-dependent CL spectra for the indented and adjacent pristine sites are shown in Fig. 4(b, c), obtained at acceleration voltages ranging from

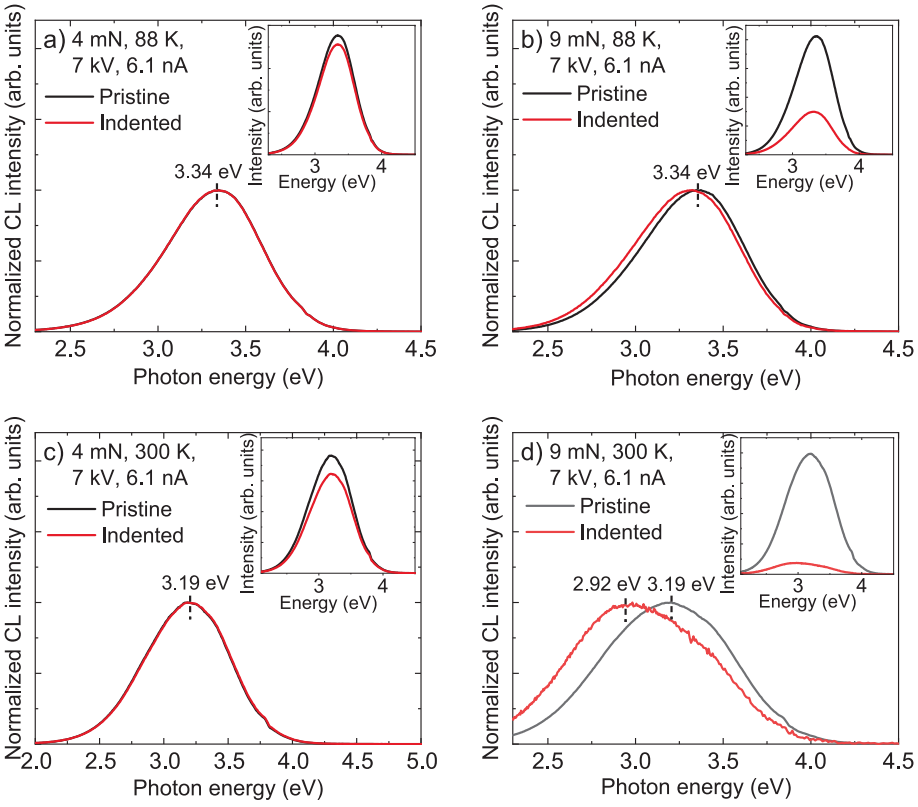

Fig. 3. Normalized CL spectra of pristine β-Ga_2O_3 crystal and indented sites at 4 mN (no pop-in) and 9 mN (with pop-in), acquired under identical electron beam excitation conditions (7 kV, 6.1nA). Insets display the corresponding as-measured CL spectra. At 4 mN, the CL spectra at 88 K and 300 K remain unchanged after indentation [panels (a, c)], indicating no additional radiative defects. At 9 mN, a large redshift from 3.19 eV to 2.92 eV at 300 K and a smaller redshift at 88 K arise from enhanced defect-related BL emission relative to the STH UV peak [panels (b, d)]. The quenching of the CL emission intensity reflects the creation of non-radiative defects due to indentation.

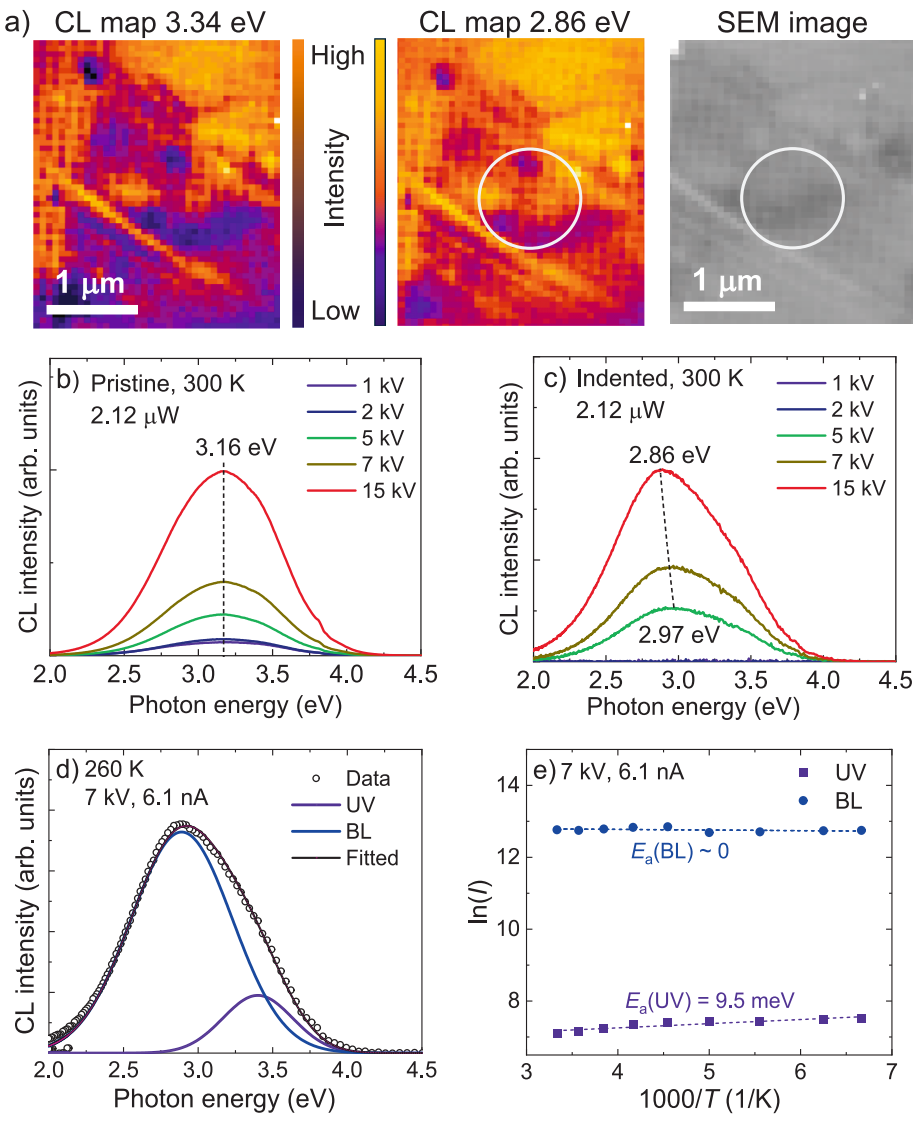

Fig. 4. (a) CL emission maps of the STH (3.34 eV) and BL (2.86 eV) emissions from the 9 mN indented site, extracted from the same hyperspectral dataset (300 K, 7 kV and 8.9 nA). The SEM image of the same area, acquired simultaneously during CL mapping, is also shown. The circle indicates the nanoindenter contact area at maximum indenter penetration depth. (b, c) Depth-dependent CL spectra acquired under 2.12 µW constant excitation from the pristine and indented regions. (d) Representative CL spectrum from the indented region, showing STH UV and defect-related BL emissions as Gaussian components. e) Arrhenius plots with linear fits, showing the thermal activation energies for the UV and BL bands.

1 to 15kV, corresponding to CL probe depths of 21–1530nm. In this depth-dependent measurement, the beam current was adjusted to maintain a constant excitation power of 2.12µW, ensuring consistent e-h pair generation at each voltage. In both pristine and indented sites, the CL intensity increases with depth, reflecting the presence of competitive non-radiative defects near the crystal surface, likely from residual polishing damage in the as-received Ga_2O_3 crystal. For the pristine site, the spectra exhibit consistent line shapes and peak positions centered at 3.16eV across all depths, confirming uniform distribution of STH and BL recombination centers. In contrast, the indented site shows a progressive redshift in the CL spectrum with depth, from 2.97 to 2.86eV [Fig. 4(c)], indicating a depth-dependent increase in vacancy defects. At low probe depths (e.g. 70nm with 2kV excitation), no CL emission is detected from the indented site, suggesting severe near-surface structural damage from nanoindentation. The CL spectrum from the indented region is dominated by the defect-related BL at 2.86eV, as illustrated in the fitted CL spectrum in Fig. 4(d). The pronounced enhancement of the BL band relative to the STH emission at the 9 mN indented site can be attributed to the generation of vacancy defects during the pop-in process [4]. While the formation of V_O and V_{Ga} defects in β-Ga_2O_3 due to nanoindentation has not been previously explored, similar luminescence enhancements have been observed in GaN, attributed to V_{Ga} defects [21]. Depth-dependent spectra with Gaussian fits from the indented site (Fig. S2) reveal that the vacancy defect densities increase sharply with depth up to 400 nm, well beyond the maximum indenter penetration depth. In contrast, the pristine β-Ga_2O_3 crystal shows negligible variation in BL emission with depth [9], confirming that the enhanced BL signal observed in the indented region arises from deformation-induced defects, rather than from undistorted material beneath the indent. This result further suggests that V_{Ga} and V_O defects are generated along dislocation slip planes activated during the pop-in event, rather than by direct contact with the indenter tip.

The application of high-pressure loads during plastic deformation or phase transformation can generate dislocations within β-Ga_2O_3. Previous studies have reported a structural phase transformation of β-Ga_2O_3 to α-Ga_2O_3 under Berkovick indentation [11]. However, in this work the Raman spectra from the indented sites show all peaks exclusively consistent with β-Ga_2O_3 (Fig. S3), confirming that the BL enhancement

results from vacancy defect generation in β-Ga_2O_3, rather than from a phase transformation. The EBSD maps in Fig. S4 provide insights into the crystallographic microstructural response of β-Ga_2O_3 under high-load indentation (10mN). Fig. S4(a) shows the EBSD band contrast (image quality) map, overlaid with the KAM map, revealing a well-defined zone of elevated local misorientation surrounding the indent, indicative of plastic strain accumulation and dislocation activity concentrated around the indent periphery [42]. Significantly, the corresponding IPF map, shown in Fig. S4(b), displays a largely uniform colour distribution outside the indentation zone, ruling out the occurrence of indentation-induced grain fragmentation or large-angle lattice rotation. These EBSD results indicate that the indentation introduces localized deformation as well as point defect and dislocation generation without causing significant crystallographic reorientation or phase transformation, consistent with the Raman and CL findings. Dislocation motion and interactions during nanoindentation are known to generate a high concentration of vacancy defects. According to established models, when the stress along a dislocation line exceeds a critical threshold, it can induce the formation of a jog (a step out of the slip plane), which then undergoes climb, leaving behind a trail of vacancies [4,43]. In β-Ga_2O_3, our results indicate that dislocation motion during the pop-in event serves a dual role: (i) it creates extended non-radiative recombination centers that suppress the STH UV emission, and (ii) it simultaneously generates vacancy defects that increase DAP-related BL emission. This interpretation is supported by spatially correlated evidence from EBSD strain maps and depth-resolved CL spectra (Figs. S4 and S2), which show localized plastic strain and increased vacancy-related emission beyond the indenter contact region. The sharp increase in BL intensity following the pop-in event indicates the formation of DAP centers associated with V_O and V_{Ga} defects, attributed to dislocation motion and stress-induced lattice rearrangement during the abrupt onset of plasticity. While the formation energies of these vacancies are high under thermal equilibrium, nanoindentation induces intense, localized stress fields that drive non-equilibrium vacancy formation, as similarly observed in other semiconductors [15,44]. This interpretation is supported by our CL and EBSD data, which reveal dislocation-mediated defect generation extending well beyond the contact zone. While positron annihilation spectroscopy (PAS) could provide additional insight into the nature of these vacancy defects, its application is currently limited by the small size of the indentation-affected zones and the lack of sufficiently focused PAS microbeam. Future studies may revisit this approach as higher spatial resolution PAS techniques become available.

Arrhenius analysis of the UV integrated intensities at the 9 mN indented site, shown in Fig. 4(e), yields a thermal activation energy (E_a) of 9.5meV. This value is comparable with the binding energies (17 – 50meV) reported for shallow Sn and Si donors, common impurities in EFG β-Ga_2O_3 crystals [45]. In contrast, the BL defect emission shows minimal temperature dependence, indicating negligible activation energy. This unusual kinetic behavior is likely due to electron tunnelling effects involving defect traps generated by indentation [46], where the local matrix surrounding vacancy defects plays a critical role. The contrasting thermal responses suggest that non-radiative recombination becomes increasingly competitive at elevated temperatures, suppressing the STH-associated UV emission, whereas the DAP-related BL recombination remains more resilient. These findings indicate that at room temperature and above, DAP transitions dominate over STH recombination pathways. Furthermore, the BL peak position remains unchanged with increasing excitation power (Fig. S5). This behavior is characteristic of deep vacancy centers where carriers are highly localized and the DAP transition involves only closely bound donor–acceptor pairs. In contrast, more common shallow donor–deep acceptor pairs with delocalized donors would exhibit a blue shift in the BL peak with increasing excitation power due to a broader range of pair separations (see Note S6 for a detailed explanation of DAP-induced BL peak shifts with increasing excitation energy). Additionally, the effects of nanoindentation are highly localized and do not alter the bulk carrier concentration of the β-Ga_2O_3 crystal, which remains at $8\times10^{17}cm^{-3}$ post-indentation.

4. Conclusion

Spherical nanoindentation experiments with applied loads up to 10 mN were performed to investigate the local mechanical properties and stability of bulk (−201) β-Ga_2O_3 crystals. Load-displacement measurements reveal pop-in events with indenter loads from 8 mN, indicating the onset of elastic–plastic deformation. CL spectroscopy after indentation show substantial quenching of the intrinsic UV emission at 3.3eV (associated with self-trapped holes) and enhanced blue luminescence (BL) at 2.9eV, attributed to deep-level donor–acceptor pair (DAP) transitions involving V_O and V_{Ga} defects. The observed 270meV redshift and intensity enhancement in the BL band are consistent with the formation of these vacancy defects during dislocation nucleation. Depth-resolved CL and EBSD analyses confirm that vacancy generation is not limited to the contact zone but extends laterally and vertically due to dislocation motion. Local misorientation patterns near the indent perimeter further support dislocation-mediated plastic flow as the dominant mechanism of defect formation, rather than thermally driven diffusion. These dislocations act both as non-radiative recombination centers, suppressing UV emission, and as sources of vacancy defects that enhance DAP BL emission. The simultaneous formation of radiative and non-radiative defects under mechanical stress highlights the structural and optoelectronic sensitivity of β-Ga_2O_3 to deformation, which is critical for its application in power and optoelectronic devices.

CRediT authorship contribution statement

Curtis P. Irvine: Writing – original draft, Methodology, Investigation, Formal analysis. **Billy J. Murdoch:** Methodology, Investigation. **Matthew R. Field:** Methodology, Investigation. **Fatima Matar:** Validation, Investigation. **Matthew R. Phillips:** Writing – review & editing, Funding acquisition, Conceptualization. **Cuong Ton-That:** Writing – review & editing, Methodology, Formal analysis, Conceptualization.

Declaration of competing interest

The authors declare that they have no known competing financial interests or personal relationships that could have appeared to influence the work reported in this paper.

Acknowledgements

The authors acknowledge the technical assistance of Herbert Yuan and Linda Xiao. This work was supported under Australian Research Council (ARC) Discovery Project funding scheme (project DP210101146).

Appendix A. Supplementary data

Supplementary data to this article can be found online at https://doi.org/10.1016/j.apsusc.2025.164217.

Data availability

Data will be made available on request.

References

[1] S.J. Pearton, J. Yang, P.H. Cary IV, F. Ren, J. Kim, M.J. Tadjer, M.A. Mastro, A review of Ga_2O_3 materials, processing, and devices, Appl. Phys. Rev. 5 (2018) 011301.
[2] A. Perez-Tomas, E. Chikoidze, Y. Dumont, M.R. Jennings, S. Russell, P. Vales-Castro, G. Catalan, M. Lira-Cantu, C. Ton-That, F.H. Teherani, Giant bulk

photovoltaic effect in solar cell architectures with ultra-wide bandgap Ga_2O_3 transparent conducting electrodes, Mater. Today Energy 14 (2019) 100350.
[3] Y. Wu, S. Gao, H. Huang, The deformation pattern of single crystal β-Ga_2O_3 under nanoindentation, Mater. Sci. Semicond. Process. 71 (2017) 321–325.
[4] J. Huang, K. Xu, Y.M. Fan, J.F. Wang, J.C. Zhang, G.Q. Ren, Dislocation luminescence in GaN single crystals under nanoindentation, Nanoscale Res. Lett. 9 (2014) 649.
[5] S. Kucheyev, J. Bradby, J. Williams, C. Jagadish, M. Swain, Mechanical deformation of single-crystal ZnO, Appl. Phys. Lett. 80 (2002) 956–958.
[6] T. Onuma, S. Fujioka, T. Yamaguchi, M. Higashiwaki, K. Sasaki, T. Masui, T. Honda, Correlation between blue luminescence intensity and resistivity in β-Ga_2O_3 single crystals, Appl. Phys. Lett. 103 (2013) 041910.
[7] Y.S. Wang, P.T. Dickens, J.B. Varley, X.J. Ni, E. Lotubai, S. Sprawls, F. Liu, V. Lordi, S. Krishnamoorthy, S. Blair, K.G. Lynn, M. Scarpulla, B. Sensale-Rodriguez, Incident wavelength and polarization dependence of spectral shifts in β-Ga_2O_3 UV photoluminescence, Sci. Rep. 8 (2018) 18075.
[8] A.K. Salih, S. Fiedler, C.P. Irvine, F. Matar, M.R. Phillips, C. Ton-That, Defect passivation and enhanced UV emission in β-Ga_2O_3 via remote fluorine plasma treatment, Appl. Surf. Sci. 687 (2025) 162250.
[9] C.P. Irvine, A. Stopic, M.T. Westerhausen, M.R. Phillips, C. Ton-That, Enhancement of excitonic and defect-related luminescence in neutron transmutation doped β-Ga_2O_3, Phys. Rev. Mater. 6 (2022) 114603.
[10] H.T. Gao, S. Muralidharan, M.R. Karim, S.M. White, L.R. Cao, K. Leedy, H.P. Zhao, D.C. Look, L.J. Brillson, Neutron irradiation and forming gas anneal impact on β-Ga_2O_3 deep level defects, J. Phys. D Appl. Phys. 53 (2020) 465102.
[11] S. Gao, X. Yang, J. Cheng, X. Guo, R. Kang, Deformation and fracture behaviors of monocrystalline β-Ga_2O_3 characterized using indentation method and first-principles calculations, Mater Charact 200 (2023) 112920.
[12] R. Yang, N. Xia, K. Ma, D. Wu, J. Wang, Z. Jin, H. Zhang, D. Yang, The anisotropy of deformation behaviors in (100) and (010) plane of monoclinic β-Ga_2O_3 single crystals, J. Alloy. Compd. 978 (2024) 173556.
[13] K. Sasaki, Prospects for β-Ga_2O_3: now and into the future, Appl. Phys Express 17 (2024) 090101.
[14] S. Wen, R. Zong, F. Zeng, S. Guo, F. Pan, Nanoindentation and nanoscratch behaviors of Ag/Ni multilayers, Appl. Surf. Sci. 255 (2009) 4558–4562.
[15] V.A. Coleman, J. Bradby, C. Jagadish, M. Phillips, Observation of enhanced defect emission and excitonic quenching from spherically indented ZnO, Appl. Phys. Lett. 89 (2006) 082102.
[16] Z. Takkouk, N. Brihi, K. Guergouri, Y. Marfaing, Cathodoluminescence study of plastically deformed bulk ZnO single crystal, Phys. B Condens. Matter 366 (2005) 185–191.
[17] S. Kucheyev, J. Bradby, J. Williams, C. Jagadish, M. Toth, M.R. Phillips, M. V. Swain, Nanoindentation of epitaxial GaN films, Appl. Phys. Lett. 77 (2000) 3373–3375.
[18] W.-H. Yau, P.-C. Tseng, H.-C. Wen, C.-H. Tsai, W.-C. Chou, Luminescence properties of mechanically nanoindented ZnSe, Microelectron. Reliab. 51 (2011) 931–935.
[19] P. Goswami, S. Pal, M. Gupta, Investigation of point defect evolution and Voronoi cluster analysis for magnesium during nanoindentation, J. Magnesium Alloys 11 (2023) 1029–1042.
[20] A. Sciuto, P.P. Barbarino, D. Mello, G. D'Arrigo, Insight on defects mechanically introduced by nanoindentation in 4H-SiC p-n diode, Mater. Des. 239 (2024) 112751.
[21] H. Lei, H.S. Leipner, J. Schreiber, J.L. Weyher, T. Wosiński, I. Grzegory, Raman and cathodoluminescence study of dislocations in GaN, J. Appl. Phys. 92 (2002) 6666–6670.
[22] M.H. Zaldívar, P. Fernández, J. Piqueras, Influence of deformation on the luminescence of GaN epitaxial films, Semicond. Sci. Technol. 13 (1998) 900.
[23] A.D. Sidiropoulos, E. Harea, A.A. Konstantinidis, E.C. Aifantis, "Pop-in" and "pop-out" effect in monocrystalline silicon. A statistical investigation, J. Mech. Behav. Mater. 26 (2017) 65–71.
[24] F. Pöhl, Pop-in behavior and elastic-to-plastic transition of polycrystalline pure iron during sharp nanoindentation, Sci. Rep. 9 (2019) 15350.
[25] J. Huang, K. Xu, Y.M. Fan, M.T. Niu, X.H. Zeng, J.F. Wang, H. Yang, Nanoscale anisotropic plastic deformation in single crystal GaN, Nanoscale Res. Lett. 7 (2012) 150.
[26] L. Zhu, M. Lockrey, M.R. Phillips, C. Ton-That, Spatial distribution of defect luminescence in ZnO nanorods: an investigation by spectral cathodoluminescence imaging, Phys. Status Solidi (a) 215 (2018) 1800389.
[27] D. Drouin, A.R. Couture, D. Joly, X. Tastet, V. Aimez, R. Gauvin, CASINO V2.42: a fast and easy-to-use modeling tool for scanning electron microscopy and microanalysis users, Scanning 29 (2007) 92–101.
[28] D. Lorenz, A. Zeckzer, U. Hilpert, P. Grau, H. Johansen, H.S. Leipner, Pop-in effect as homogeneous nucleation of dislocations during nanoindentation, Phys. Rev. B 67 (2003) 172101.
[29] K. Tao, X. He, H. Lu, Z. Zhang, Y. Yang, E. Pineda, K. Song, Y. He, J. Qiao, Model for the onset of plasticity and hardness in bulk metallic glasses investigated by nanoindentation with a spherical indenter, Int. J. Solids Struct. 310 (2025) 113238.
[30] W.C. Oliver, G.M. Pharr, An improved technique for determining hardness and elastic modulus using load and displacement sensing indentation experiments, J. Mater. Res. 7 (1992) 1564–1583.
[31] W.C. Oliver, G.M. Pharr, Measurement of hardness and elastic modulus by instrumented indentation: advances in understanding and refinements to methodology, J. Mater. Res. 19 (2004) 3–20.
[32] J.S. Field, M.V. Swain, A simple predictive model for spherical indentation, J. Mater. Res. 8 (1993) 297–306.
[33] T. Hou, W. Zhang, W. Mu, C. Li, X. Li, X. Ma, J. Zhang, H. Wang, Z. Jia, D. Liu, X. Tao, The anisotropy dependence of deformation mechanism of cleavage planes in β-Ga_2O_3 single crystal, Mater. Sci. Semicond. Process. 158 (2023) 107357.
[34] J. Liu, H. Deng, X. Zhao, C. Wu, H. Zhang, F. Lang, Investigation of the nano and micromechanical performance of β-Ga_2O_3 epitaxial films on sapphire using nanoindentation, Vacuum 227 (2024) 113413.
[35] K. Durst, M. Göken, G.M. Pharr, Indentation size effect in spherical and pyramidal indentations, J. Phys. D Appl. Phys. 41 (2008) 074005.
[36] Z. Jin, P. Lv, Y. Xu, Y. Li, Q. Dong, G. Xiao, B. Zou, Blue light emission enhancement and robust pressure resistance of gallium oxide nanocrystals, Chem. Sci. 15 (2024) 11367–11373.
[37] M. Maruzane, Y. Oshima, O. Makydonska, P.R. Edwards, R.W. Martin, F. C. Massabuau, Luminescence properties of dislocations in α-Ga_2O_3, J. Phys. D Appl. Phys. 58 (2024) 03LT02.
[38] J. Lähnemann, V.M. Kaganer, K.K. Sabelfeld, A.E. Kireeva, U. Jahn, C. Chèze, R. Calarco, O. Brandt, Carrier diffusion in GaN: a cathodoluminescence study. III. Nature of nonradiative recombination at threading dislocations, Phys. Rev. Appl 17 (2022) 024019.
[39] K. Yamamura, L. Zhu, C.P. Irvine, J.A. Scott, M. Singh, A. Jallandhra, V. Bansal, M. R. Phillips, C. Ton-That, Defect compensation in nitrogen-doped β-Ga_2O_3 nanowires: implications for bipolar nanoscale devices, ACS Appl. Nano Mater. 5 (2022) 12087–12094.
[40] F. Matar, Y.-L. Shi, F.-C.-C. Ling, A. Salih, C.P. Irvine, S. De Silva, M.R. Phillips, C. Ton-That, Bandgap narrowing and hole self-trapping reduction in Ga_2O_3 by Bi_2O_3 alloying, J. Alloy. Compd. 960 (2023) 170983.
[41] S.-R. Jian, I.J. Teng, J.-M. Lu, Cathodoluminescence and cross-sectional transmission electron microscopy studies for deformation Behaviors of GaN Thin Films under Berkovich nanoindentation, Nanoscale Res. Lett. 3 (2008) 158.
[42] M. Seehaus, S.-H. Lee, T. Stollenwerk, J.M. Wheeler, S. Korte-Kerzel, Estimation of directional single crystal elastic properties from nano-indentation by correlation with EBSD and first-principle calculations, Mater. Des. 234 (2023) 112296.
[43] J. Čížek, M. Janeček, T. Vlasák, B. Smola, O. Melikhova, I.rk, d.sv, The development of vacancies during severe plastic deformation, Mater. Trans. 60 (2019) 1533–1542.
[44] J.E. Bradby, S.O. Kucheyev, J.S. Williams, J. Wong-Leung, M.V. Swain, P. Munroe, G. Li, M.R. Phillips, Indentation-induced damage in GaN epilayers, Appl. Phys. Lett. 80 (2002) 383–385.
[45] A.T. Neal, S. Mou, S. Rafique, H.P. Zhao, E. Ahmadi, J.S. Speck, K.T. Stevens, J. D. Blevins, D.B. Thomson, N. Moser, K.D. Chabak, G.H. Jessen, Donors and deep acceptors in β-Ga_2O_3, Appl. Phys. Lett. 113 (2018) 062101.
[46] B. Ershov, F. Kieffer, Effect of temperature on recombination luminescence and electron tunnelling, Nature 252 (1974) 118–119.